JOURNAL OF APPLIED CRYSTALLOGRAPHY

ISSN 1600-5767

Growth and annealing kinetics of α-sexithiophene and fullerene C_{60} mixed films

Christopher Lorch,[a] Katharina Broch,[b] Valentina Belova,[a] Giuliano Duva,[a] Alexander Hinderhofer,[a] Alexander Gerlach,[a] Maciej Jankowski[c] and Frank Schreiber[a]*

[a]Institut für Angewandte Physik, Universität Tübingen, Auf der Morgenstelle 10, 72076 Tübingen, Germany, [b]Cavendish Laboratory, Department of Physics, University of Cambridge, Cambridge CB3 0HE, UK, and [c]ESRF – The European Synchrotron, 71 Avenue des Martyrs, 38000 Grenoble, France. *Correspondence e-mail: frank.schreiber@uni-tuebingen.de

Received 8 February 2016
Accepted 18 June 2016

Edited by A. R. Pearson, Universität Hamburg, Germany

Keywords: fullerene; sexithiophene; real-time studies; annealing; thin-film growth.

Supporting information: this article has supporting information at journals.iucr.org/j

Thin films of α-sexithiophene (6T) and C_{60} mixtures deposited on nSiO substrates at 303 and 373 K were investigated in real time and *in situ* during the film growth using X-ray diffraction. The mixtures are observed to contain the well known 6T low-temperature crystal phase and the β phase, which usually coexist in pure 6T films. The addition of C_{60} modifies the structure to almost purely β-phase-dominated films if the substrate is at 303 K. In contrast, at 373 K the low-temperature crystal phase of 6T dominates the film growth of the mixtures. Post-growth annealing experiments up to 373 K on equimolar mixtures and pure 6T films were also performed and followed in real time with X-ray diffraction. Annealing of pure 6T films results in a strong increase of film ordering, whereas annealing of equimolar 6T:C_{60} mixed films does not induce any significant changes in the film structure. These results lend further support to theories about the important influence of C_{60} on the growth behaviour and structure formation process of 6T in mixtures of the two materials.

1. Introduction

Organic semiconductors offer plenty of possibilities in the field of organic electronics (Brütting & Adachi, 2012; Witte & Wöll, 2004; Forrest, 2004; Deibel & Dyakonov, 2010; Tsutsui & Fujita, 2002), in particular for organic photovoltaics. However, the structure–function relationship in molecular systems is more complex in comparison to atomistic systems because of additional degrees of freedom (orientation) and the weak interaction potentials (van der Waals forces). The thin-film structure, organic–organic interfaces and domain sizes all play an important role (Witte & Wöll, 2004; Schreiber, 2004; Opitz *et al.*, 2010; Pivrikas *et al.*, 2007; Poelking *et al.*, 2015; Rand *et al.*, 2005; Nolasco *et al.*, 2010). The active layer of organic solar cells generally utilizes at least two different organic compounds (a donor material and an acceptor material), which are employed in a planar structure with the acceptor on top of the donor (or *vice versa*), so-called planar heterojunctions (PHJs), or in blended bulk heterojunctions (BHJs). For the latter, the mixed system can follow different scenarios, depending on growth parameters, interaction energies and steric compatibilities (Hinderhofer & Schreiber, 2012). Either the materials mix on a molecular level forming new ordered structures (Broch, Gerlach *et al.*, 2013) or a statistical mixture (Broch, Aufderheide *et al.*, 2013; Aufderheide *et al.*, 2012), or the materials phase separate into domains of the pristine materials (Salzmann *et al.*, 2008; Wagner *et al.*, 2010; Hinderhofer & Schreiber, 2012). For a broader overview of the field

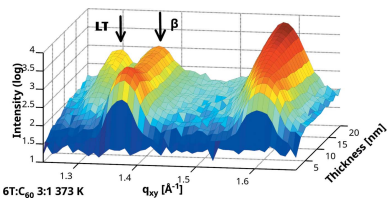

of organic thin-film growth and characterization see Witte & Wöll (2004), Rivnay *et al.* (2012), Jones *et al.* (2016), Desai *et al.* (2011), Moulin *et al.* (2006) and Yang *et al.* (2015).

The material combination α-sexithiophene ($C_{24}H_{14}S_6$, 6T) and Buckminster fullerene C_{60} (Figs. 1*a* and 1*b*) can be employed as a donor–acceptor pair in the PHJ geometry (Hörmann *et al.*, 2011) as well as in BHJs (Veenstra *et al.*, 1997; Sakai *et al.*, 2008). For PHJs, interesting effects of the mutual arrangement and orientation of the two materials on the open-circuit voltage have been reported (Hörmann *et al.*, 2014). For BHJ devices with 6T and either C_{60} or C_{70}, an improvement of the solar cell device parameters upon annealing is found (Alem *et al.*, 2006; Sakai *et al.*, 2009). Several studies have shown that this kind of post-growth treatment can be employed to modify device parameters (Peumans *et al.*, 2003; Yang *et al.*, 2005; Hamilton *et al.*, 2010), including optical properties (Prabakaran *et al.*, 2002; Heutz *et al.*, 2003) as well as the structure (Ye *et al.*, 2010; Nothaft & Pflaum, 2008; Hinderhofer *et al.*, 2012). Pure 6T tends to grow in crystal structures which differ for the thin film and the single crystal (Siegrist *et al.*, 1995; Servet *et al.*, 1993, 1994; Horowitz *et al.*, 1995; Haber *et al.*, 2008; Simbrunner *et al.*, 2011). In thin films, 6T mostly adopts two different crystal structures in 'standing-up' orientations, either the low-temperature single-crystal phase (LT phase) (Horowitz *et al.*, 1995) or the β phase (Servet *et al.*, 1993, 1994). Coexistence of both phases in thin films has also been observed (Moser *et al.*, 2013; Lorch *et al.*, 2015). The LT phase is dominant for low deposition rates or at elevated substrate temperature (373 K), whereas the β phase dominates at higher deposition rates and at low substrate temperatures (233 and 308 K) (Moser *et al.*, 2013; Lorch *et al.*, 2015). Generally, the β phase is formed close to the substrate, and above a certain thickness a transition to growth dominated by the LT phase occurs (Lorch *et al.*, 2015). The β phase is energetically less stable compared to the LT phase, but is kinetically favoured (Moser *et al.*, 2013; Lorch *et al.*, 2015). The rotational symmetry of C_{60} at room temperature (Zhang *et al.*, 1991) simplifies the possible growth scenarios, because there are no different orientations, *i.e.* standing-up *versus* lying-down molecules. Thin films of C_{60} are found to show low

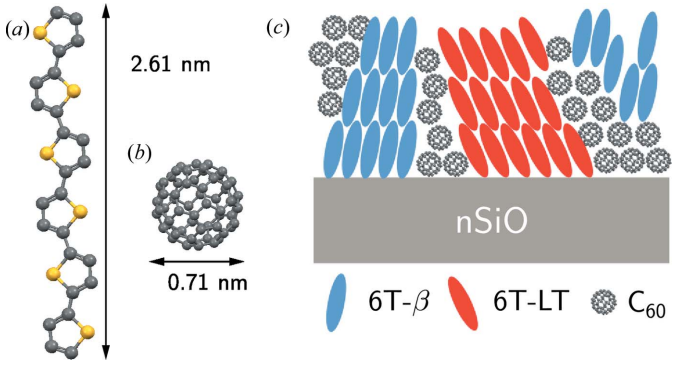

Figure 1
Schematics of (*a*) the 6T molecule [size from Horowitz *et al.* (1995)] and (*b*) the C_{60} molecule [size from Yannoni *et al.* (1991) and Adams *et al.* (1991)]. (*c*) Schematic of the mixing of 6T and C_{60}, with the two different crystal phases that are observed in the growth of the mixtures indicated.

structural order on inorganic substrates such as SiO_2 (Singh *et al.*, 2007), quartz glass (Yim & Jones, 2009) and sapphire (Itaka *et al.*, 2006). However, on organic layers like pentacene (Itaka *et al.*, 2006; Salzmann *et al.*, 2008), diindenoperylene (Hinderhofer *et al.*, 2013) or sexiphenyl (Chen *et al.*, 2008; Zhong *et al.*, 2011) an enhanced crystallinity of C_{60} layers is reported, similar to templating layers of 6T (Hörmann *et al.*, 2014).

In order to characterize the mixing behaviour of C_{60} and 6T we performed real-time *in situ* grazing-incidence X-ray diffraction (GIXD) experiments. The films were characterized post-growth, using X-ray reflectivity (XRR), wide-range GIXD scans and reciprocal space maps. After detailed post-growth characterization, the films were annealed in order to investigate structural changes. Performing the experiments directly under high vacuum conditions ensures that effects such as degradation of the structure or incorporation of impurities due to the exposure to ambient conditions are excluded. Furthermore, transient effects can only be identified if the growth is followed directly in real time (Banerjee *et al.*, 2013; Bommel *et al.*, 2014; Kowarik *et al.*, 2006; Heinemeyer *et al.*, 2010; Krause *et al.*, 2004; Liscio *et al.*, 2013; Kowarik *et al.*, 2008; Brock *et al.*, 2010). Films with three different mixing ratios were prepared. Nominally, the molecular ratios were set to 6T:C_{60} 3:1, 1:1 and 1:3. All films were grown at 303 or 373 K substrate temperature. As reference samples, films of the pure materials were prepared. In the following, we will refer to the data as 6T:C_{60} (*m*:*n*) 303 K (373 K) for the different ratios (*m*:*n*) prepared at different substrate temperatures. Depending on the substrate temperature, either the 6T LT phase or the 6T β phase dominates the growth, whereas C_{60} grows mainly in randomly oriented domains (Fig. 1*c*).

2. Experimental

6T was purchased from Sigma Aldrich and purified twice by temperature gradient sublimation. C_{60} was purchased from Creaphys and used without further purification. The samples were prepared and studied in a portable vacuum chamber ($p = 1 \times 10^{-8}$ mbar = 1 µPa) (Ritley *et al.*, 2001). Before the installation, silicon (nSiO) substrates with a native oxide layer of 2.0 nm were cleaned in an ultrasonic bath with acetone, 2-propanol and demineralized water. Before each sample preparation the substrates were heated to 770 K to desorb the previously grown film. Deposition rates between 0.3 and 0.5 nm min^{-1} were monitored using a water-cooled quartz crystal microbalance (QCM), which was calibrated *via* XRR. The nominal thickness of all films was 20 nm. The molecules were evaporated from two independent, thermally shielded Knudsen cells. The evaporation temperatures of the different mixing ratios are summarized in Table 1.

The nSiO substrates were mounted on a molybdenum sample holder, cooled by liquid nitrogen or heated resistively when needed. The substrate temperature was monitored using a K-type thermocouple attached to the sample holder in close proximity to the substrates. All samples were measured at the same temperature as prepared. All experiments were

Table 1
Evaporation temperatures for the different mixing ratios.

Mixing ratio	6T temperature (K)	C_{60} temperature (K)
Pure 6T	527	n.a.
6T:C_{60} 3:1	527	635
6T:C_{60} 1:1	521	651
6T:C_{60} 1:3	515	659
Pure C_{60}	n.a.	663

performed at the ID03 beamline at the European Synchrotron Radiation Facility (ESRF) using a monochromatic X-ray beam at 20.0 keV (wavelength 0.6199 Å). Diffraction images were recorded using a MaxiPix area detector (Ponchut *et al.*, 2011). Slits directly in front of the detector were used to mimic a point detector where needed. For the qualitative peak analysis no instrumental broadening is included in the calculations; therefore the reported values for the coherently scattering grain sizes are lower limits. The critical angle of nSiO is $\alpha_c = 0.08°$ at a photon energy of 20 keV. To obtain maximum surface sensitivity, we chose an incidence angle of $\alpha_i = 0.075°$ for the measurements. The time difference between the start of two successive real-time GIXD scans was 260 s. With the deposition rates used, this results in a 1.3–2.1 nm thickness resolution. For further analysis, two-dimensional reciprocal space maps were recorded with fully open detector slits.

3. Results and discussion

3.1. X-ray reflectivity

XRR was used to investigate the out-of-plane structure of the 6T:C_{60} mixed and pure films. Fig. 2(*a*) depicts the data obtained for the films prepared at a substrate temperature of

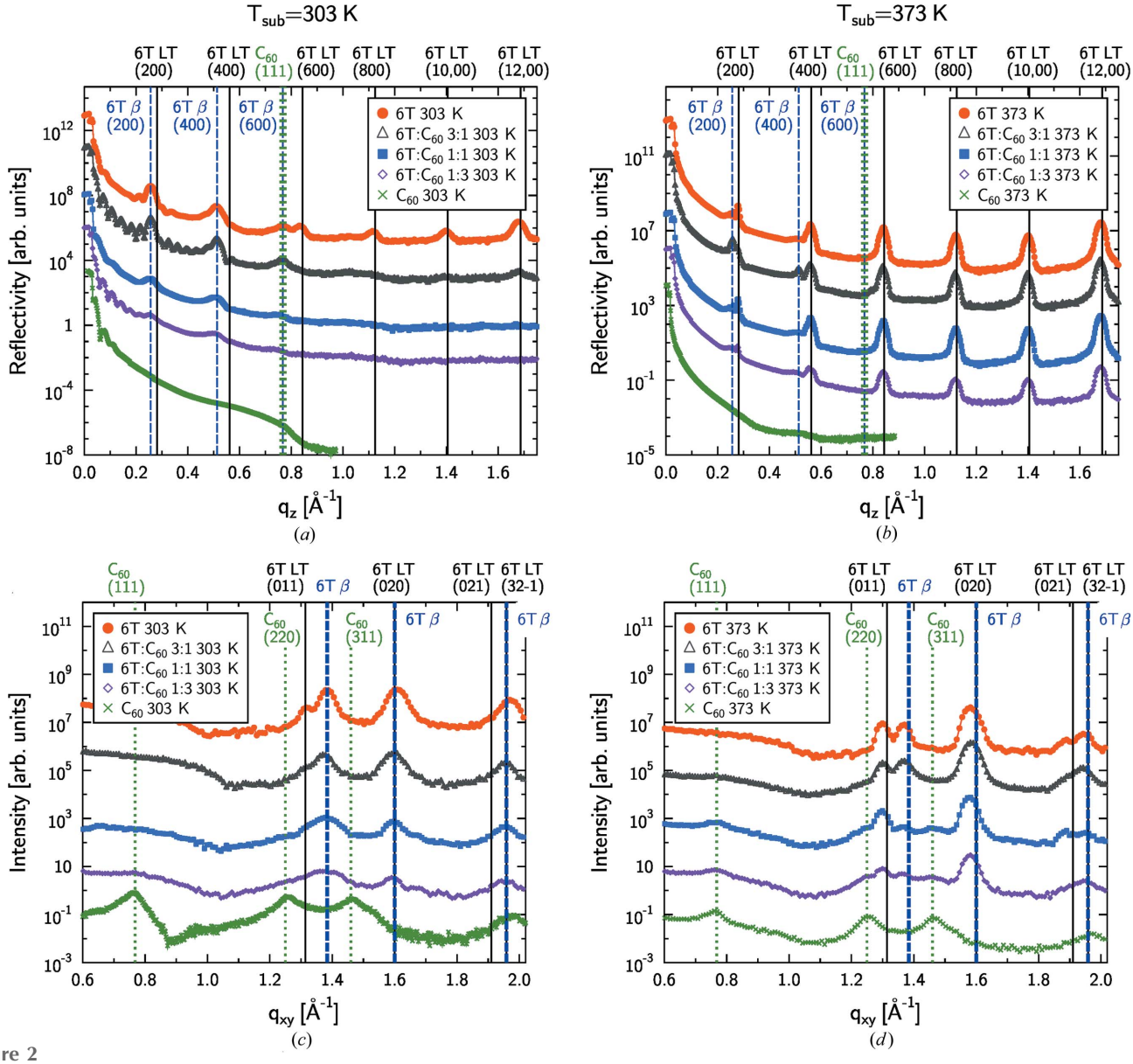

Figure 2
(*a*), (*b*) XRR data and (*c*), (*d*) GIXD data for different mixing ratios at (*a*), (*c*) 303 K and (*b*), (*d*) 373 K substrate temperature.

303 K. The structure of the pure 6T film at 303 K is consistent with that reported previously (Lorch *et al.*, 2015). The out-of-plane structure shows features belonging to the β phase as well as the LT phase: in particular, Bragg peaks of the standing-up oriented LT phase up to the 12th order. Under the applied preparation conditions, pure C_{60} does not form a well ordered out-of-plane structure, since no characteristic out-of-plane reflections of C_{60} are observed. All Bragg peaks seen for the mixtures prepared at 303 K originate from 6T domains (Horowitz *et al.*, 1995; Servet *et al.*, 1993, 1994).

For the 6T:C_{60} (3:1) 303 K mixture the first six orders of the Bragg reflections corresponding to the β phase are clearly visible (Servet *et al.*, 1993, 1994). Note that the 6T β 600 reflection is found at the identical q_z value as the C_{60} 111 reflection (Krätschmer *et al.*, 1990). However, since the mixture contains significantly more 6T, and in the other mixtures with a higher amount of C_{60} this feature is not as pronounced, it is very likely that this peak can be assigned to the 6T β phase. A slight distortion of the 6T β 400 peak and a small hump at the position of the 12 0 0 peak of the LT phase, indicate that there are still small fractions of the LT phase within the film. With increasing fraction of C_{60} in the mixtures the crystallinity of 6T decreases further. For both 6T:C_{60} (1:1) 303 K and 6T:C_{60} (1:3) 303 K, the 200, 400 and 600 Bragg peaks of the β phase are very weak. There are no more indications of any well ordered out-of-plane crystallites of the LT phase in these mixtures. The Kiessig oscillations in a q_z range up to around 0.2 Å^{-1} stem from interference from scattering from the top of the film surface and the surface of the substrate (Kiessig, 1931; Als-Nielsen & McMorrow, 2011). These oscillations are damped out with an increasing roughness of the films (Als-Nielsen & McMorrow, 2011). At 303 K, the non-equimolar mixtures, in particular, exhibit very pronounced oscillations, indicating very smooth films. This might be explained by C_{60} filling the voids between the 6T domains or *vice versa*, similar to results for perfluoropentacene deposited on diindenoperylene or pentacene on perfluoropentacene, where a small step edge barrier leads to a smoothing of the bottom layer when an overlayer is deposited on top (Hinderhofer *et al.*, 2010).

The films prepared at a substrate temperature of 373 K (Fig. 2*b*) all show, with the exception of pure C_{60}, a higher crystallinity compared to those prepared at 303 K. In contrast to the low-temperature films, for all films the 6T LT phase dominates over the 6T β phase. Pronounced Bragg peaks corresponding to the LT phase are clearly visible up to approximately $q_z = 1.7$ Å^{-1}. By fitting the 12 0 0 and 10 0 0 reflections and using Scherrer's equation ($D_{\rm coh} = 2\pi K/$ FWHM, with $K = 0.94$ for spherical crystallites, FWHM being the full width at half-maximum of the fitted peaks) to estimate the coherently scattering crystal size $D_{\rm coh||}$ (Scherrer, 1918), one obtains values of ~20 nm, corresponding very well to the nominal film thickness. This indicates the presence of crystals with an extension over the whole film thickness. In contrast to the low-temperature films, almost no Bragg reflections arising from the β phase are visible. Only the 6T:C_{60} (3:1) 373 K mixture shows the first four orders of the Bragg peaks of the β phase. For all the films no Kiessig oscillations are observable, indicating that the surface roughness is significantly greater than in the low-temperature films.

3.2. Grazing incidence diffraction

GIXD measurements were performed to identify and characterize the in-plane crystalline structure of the films. The data for a substrate temperature of 303 K are plotted in Fig. 2(*c*). The peaks of all films can be clearly attributed to either 6T or C_{60}. Considering these results together with the

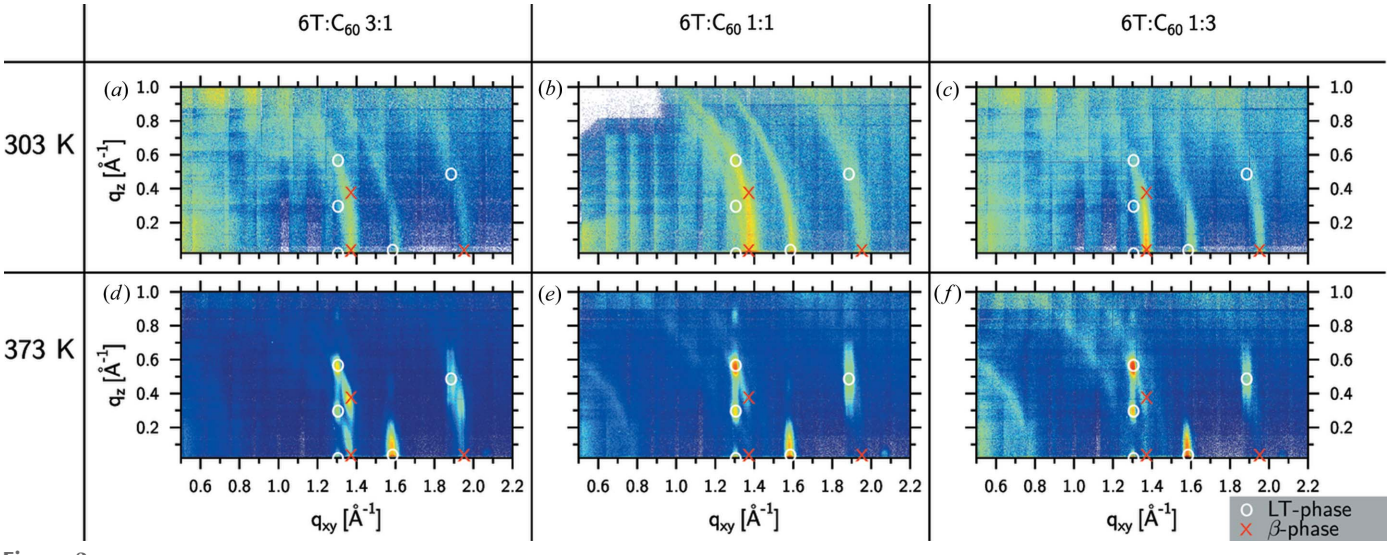

Figure 3
Two-dimensional reciprocal space maps of six different 6T:C_{60} mixtures. In the mixtures prepared at low substrate temperatures [(*a*)–(*c*), top row] the peaks of 6T are smeared out and not very well defined. The rings usually seen for C_{60} (Fig. 8 in the supporting material) are not observed, since their signal is rather low. In the mixtures prepared at high substrate temperature [(*d*)–(*f*), bottom row] the 6T peaks are relatively well defined. In the 6T:C_{60} (1:1) and (1:3) mixtures [(*e*) and (*f*), respectively], weak rings arising from C_{60} are visible. The images were taken with a MaxiPix area detector and are composed of 147 single pictures combined using the *BINoculars* software (Roobol *et al.*, 2015; Drnec *et al.*, 2014).

XRR data (Fig. 2*a*), we conclude that the two materials do not form a new crystal structure. The Bragg peaks of the pure materials within the mixtures indicate that there are separated domains of the pure materials. The GIXD data of the pure 6T 303 K are dominated by β-phase domains. The data of pure C_{60} exhibit only reflections belonging to the C_{60} face-centred cubic structure (Krätschmer *et al.*, 1990). Furthermore, two-dimensional area images of the scattering patterns (Fig. 8 in the supporting information) show well defined rings with constant q values, indicating a polycrystalline structure of this film.

The GIXD data of the mixtures are dominated by features from 6T (Figs. 2*c* and 3*a*–3*c*). With increasing amounts of C_{60} all 6T peaks become broader, indicating that $D_{coh||}$ decreases. In the two-dimensional GIXD data of the 303 K mixtures (Figs. 3*a*–3*c*) all diffraction peaks are smeared out relatively strongly, indicating randomly oriented domains with no preferred orientation. Overall, no reflections stemming from C_{60} can be observed.

The GIXD data of the films prepared at 373 K differ significantly from the data of the 303 K films. In general, all peaks arising from 6T (independent of the mixing ratio and the crystal structure) are shifted slightly to lower q values. We previously reported the same effect for pure 6T (Lorch *et al.*, 2015). This shift might be explained by slightly distorted, more upright standing molecules forming a slightly expanded unit cell. In the pure 6T film the structure is dominated by the LT phase with small fractions of the β phase present. The relative amount of β phase in 6T decreases with larger C_{60} fraction. The reciprocal space maps of the high-temperature mixtures (Figs. 3*d*–3*f*) show well defined 6T peaks. For 6T:C_{60} (1:1) and (1:3) weak rings stemming from C_{60} are visible, indicating that the C_{60} crystallites are randomly oriented, as in the pure C_{60} film.

3.3. Real-time grazing-incidence diffraction

We performed real-time GIXD measurements to follow and characterize the film growth *in situ*. The results for the 373 K mixtures are shown in Fig. 4. These experiments allow us to determine the thicknesses (estimated from the growth time and the measured QCM rate) at which the first domains of a certain crystal structure are formed. These values are summarized in Table 2 in the column t_{domain}. Since each real-time scan took around 260 s the values listed are upper limits and the domain formation may start earlier. The thickness at which phase separation begins can be seen as an indicator of whether the process is kinetically limited, as reported for diindenoperylene:C_{60} mixtures (Banerjee *et al.*, 2013), or not.

For 6T:C_{60}, there is only a small difference between the 303 and 373 K films. For the 303 K films the thickness at which the formation of separated 6T domains starts is 1.0–1.4 nm, and for the 373 K films it is 0.5–1.2 nm. These thicknesses are lower than the van der Waals length of a single 6T molecule (~2.6 nm) (Horowitz *et al.*, 1995; Djuric *et al.*, 2012). Taking this together with the observation that the domains formed almost exclusively have a standing-up configuration, we conclude that in the first monolayer crystal domains are already formed. This indicates that the phase separation between 6T and C_{60} starts from the beginning of the film growth and hence is probably not kinetically limited.

Table 2
Parameters of the 6T:C_{60} mixtures.

T is the substrate temperature during the growth. t_{domain} is the thickness beyond which domains of a certain crystal structure can be identified, *i.e.* a peak is clearly seen to emerge over the background level. t_{phase} is the thickness at which the intensity of the β phase starts to decrease and hence the transformation into the LT phase starts. t_{domain} and t_{phase} are extracted from the real-time GIXD data. $D_{coh||}$ is the coherently scattering in-plane domain size of the 6T 011 LT peak, the 6T β peak at ~1.38 Å^{-1} and the C_{60} 111 reflection. The highest values of $D_{coh||}$ derived from the peak width (18.3 nm for the 6T 011 LT peak and 16.8 nm for the 6T β peak) are close to the resolution limit and $D_{coh||}$ might actually be larger in these cases. n.a. indicates that the corresponding reflections were not observed.

	Mixing ratios				$D_{coh\|\|}$(nm)		
T (K)	6T	C_{60}	t_{domain} (nm)	t_{phase} (nm)	6T 011 LT	6T β	C_{60} 111
303	1	0	1.1	n.a.	15.9	14.9	n.a.
303	3	1	1.0	n.a.	14.0	11.6	n.a.
303	1	1	1.4	n.a.	n.a.	6.6	n.a.
303	1	3	1.3	n.a.	n.a.	8.4.	n.a.
303	0	1	n.a.	n.a.	n.a.	n.a.	9.3
373	1	0	1.0	n.a.	18.3	16.8	n.a.
373	3	1	1.2	4.5	18.2	12.2	n.a.
373	1	1	0.6	4.0	16.1	15.8	11.9
373	1	3	0.5	4.5	16.1	7.0	6.1
373	0	1	n.a.	n.a.	n.a.	n.a.	10.4

For the 373 K mixtures the peak corresponding to the β phase first increases and, after a certain film thickness is reached, starts to decrease. Together with this decrease, the intensity of the 6T 011 LT peak starts to increase. From the simultaneous occurrence of the two effects, we conclude that there is a transformation of already existing domains of the β phase into domains of the LT phase. The thicknesses at which this effect starts are also listed in Table 2, in the column t_{phase}. This effect occurs, independently of the mixing ratio, at a total film thickness of approximately 4 nm, which corresponds to the second monolayer of 6T.

3.4. Annealing of 1:1 mixtures and pure 6T

A common method to improve film quality after growth is to anneal the film. The 6T:C_{60} (1:1) 303 K film was heated linearly from 303 to 373 K over a period of 20 min. This temperature was maintained for 20 min and then further linearly increased to 393 K. The final temperature was kept for 120 min. Figs. 5(*a*) and 5(*c*) depict the XRR and GIXD data of the film before and after annealing, respectively. The data for the mixture prepared at 373 K are plotted as a reference. The out-of-plane data (Fig. 5*a*) indicate that the intensity of peaks corresponding to the β phase decreases slightly during heating. Similar results are obtained from the GIXD data (Fig. 5*b*). Also here, features from the β phase are less pronounced after the annealing steps. However, no significant change in the crystallinity of the films is observed after annealing.

Similar to the mixture, the 303 K pure 6T film was heated from 303 to 373 K. This increase took 20 min. Fig. 6 shows real-time GIXD scans during the annealing procedure. The exact annealing settings and times were as follows: Scan number 1 corresponds to the film just before the start of the annealing process. The time delay between scan number 1 and 2 was 20 min, during which the temperature was increased linearly from 303 to 373 K. From scan number 2 to 7, the time between each scan was 5 min and the temperature was held constant at 373 K. Scan number 8 corresponds to the scan after annealing. The gap between scan 7 and scan 8 is approximately 50 min, because of the need for an additional post-growth characterization.

While the substrate was heated from 303 to 373 K, the intensity of the peak at $q_{xy} = 1.38$ Å^{-1}, corresponding to the β phase, decreased significantly. At the same time the 6T LT 011 and the 6T LT 020 peaks markedly evolved. This indicates a transformation from β-phase crystallites into LT-phase crystallites, which are energetically more stable but whose formation is kinetically limited during the growth at low substrate temperatures. This evolution continued throughout the real-time measurements during the annealing. The peaks of the single scans were fitted with pseudo-Voigt functions and $D_{\mathrm{coh}||}$ (described above) and the intensity (area under the curve) of the different peaks were extracted. Fig. 6(*b*) shows the data as a function of time. $D_{\mathrm{coh}||}$ of the β peak (solid blue lines with filled blue dots) decreases linearly with time. After 95 min the β-phase peak vanishes completely. $D_{\mathrm{coh}||}$ of the LT 011 peak does not change during the annealing process. However, since the resolution limit of the setup is very close to

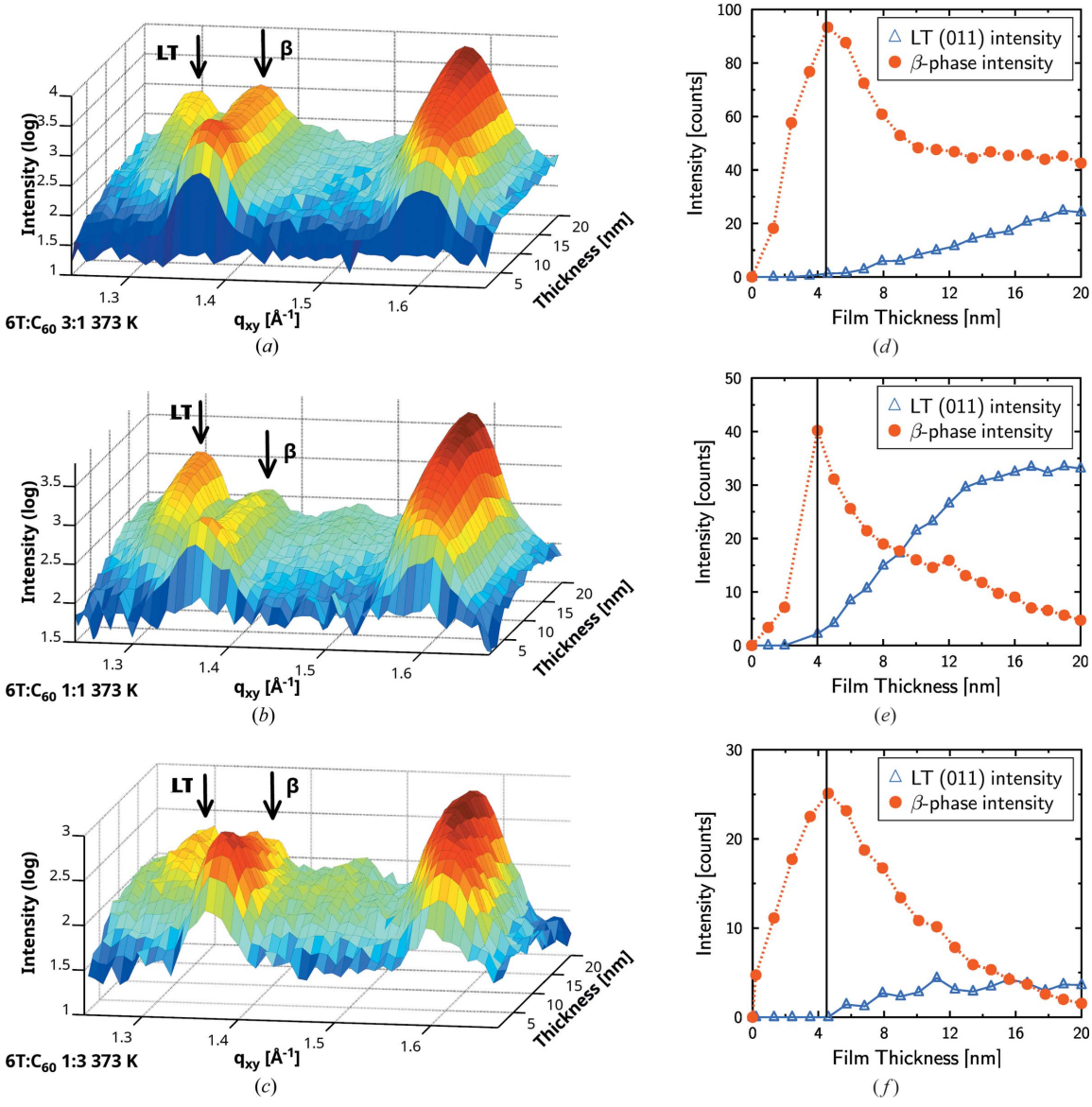

Figure 4
Real-time GIXD scans measured during film growth at 373 K. (*a*) 6T:C$_{60}$ (3:1) mixture, (*b*) 6T:C$_{60}$ (1:1) mixture and (*c*) 6T:C$_{60}$ (1:3) mixture. (*d*)–(*f*) Evolution of the intensities of the Bragg peaks corresponding to the LT 011 reflection and the β-phase reflection at $q_{xy} = 1.38$ Å^{-1} for the different mixing ratios presented on the left-hand side.

the measured result, $D_{coh||}$ of the LT phase might be larger. The intensity of this peak increases over time, indicating a transformation of the β phase into the LT phase.

In Figs. 5(*b*) and 5(*d*) the XRR and GIXD data, respectively, of the pure 6T film before and after the annealing procedure, as well as data of a film prepared at a substrate temperature of 373 K, are shown. By comparing the XRR data before and after annealing, an enhancement of the out-of-plane crystallinity together with the transition of domains from the β to the LT phase is immediately apparent. Even more remarkable is the comparison of the annealed film with the one prepared at elevated temperature. In the XRR data of the annealed film, the β-phase 200 and 400 peaks are less pronounced than those for the film prepared at 373 K. This is in agreement with the GIXD data of the films (Fig. 5*d*). Again, the peaks corresponding to the β phase vanish almost completely upon annealing. As mentioned earlier, the 6T LT-phase and β-phase unit cells can be slightly modified. In contrast to the film prepared at 373 K, this effect is less pronounced for the annealed films. This is visible in Fig. 5(*d*) where the peaks of the LT phase in the annealed film are less shifted compared to the ones observable for the film prepared at 373 K.

3.5. Discussion

The post-growth X-ray diffraction measurements for the 6T:C_{60} mixtures reveal interesting results. In general, C_{60} is not

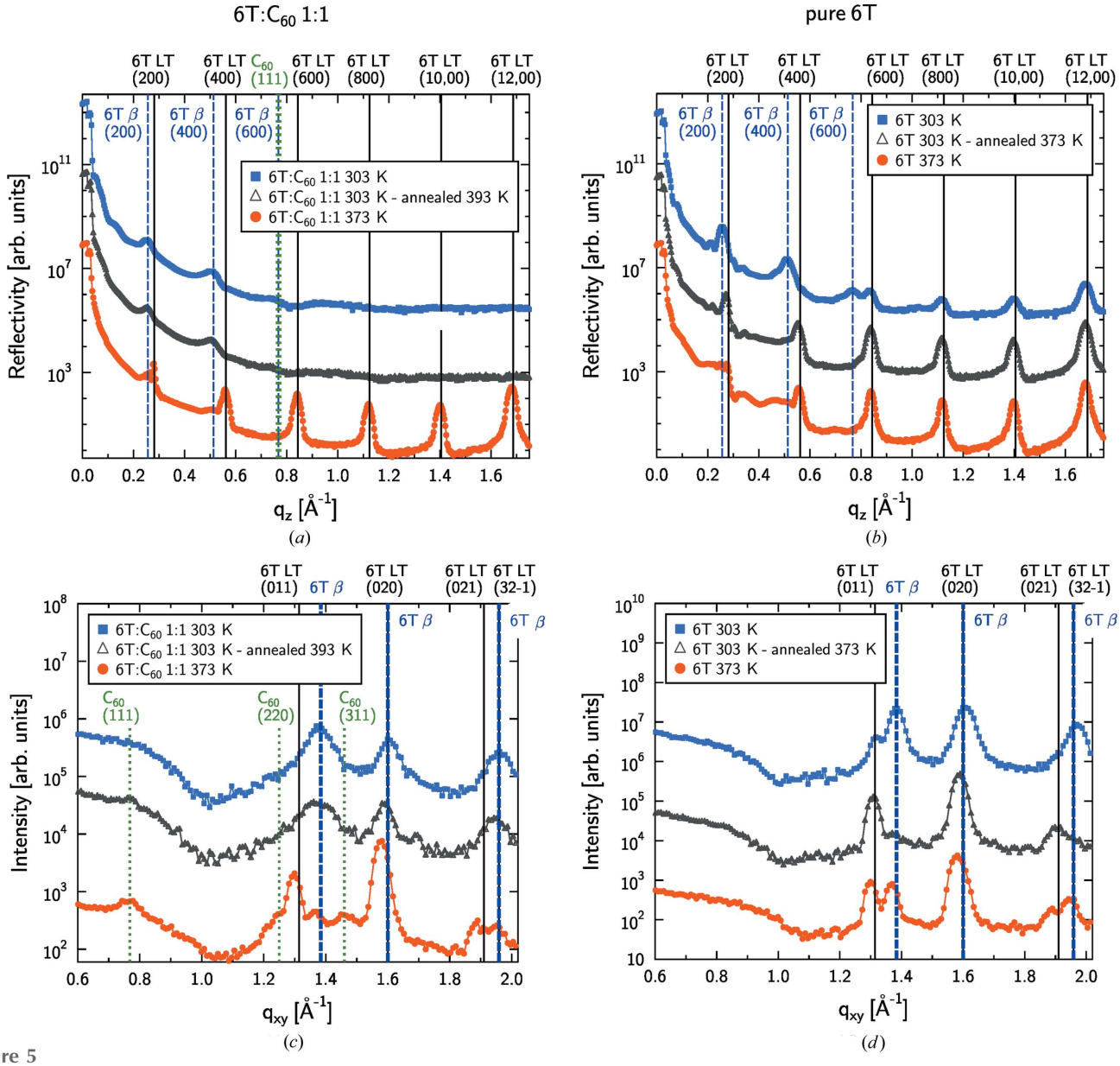

Figure 5
(*a*) XRR and (*c*) GIXD data of a 6T:C_{60} (1:1) film grown at a substrate temperature of 303 K (blue filled squares), the same film annealed at 393 K (black open triangles) and a film prepared directly at a substrate temperature of 373 K. (*b*) XRR and (*d*) GIXD data of a 6T film grown at a substrate temperature of 303 K (blue filled squares), the same film annealed at 373 K (black open triangles) and a film prepared directly at a substrate temperature of 373 K.

well ordered in any mixture investigated here. This is surprising, since in other mixed systems of C_{60} and the rod-like molecule diindenoperylene, the C_{60} phase forms relatively well ordered domains (Banerjee *et al.*, 2013). In general, the kinetic energies which the molecules have after reaching the substrate play a very important role for the growth (Schreiber, 2004; Kowarik *et al.*, 2008). This kinetic energy might be distributed and shifted between the molecules in the film and help to form different structures. Furthermore, other kinds of external influences, like optical heating, can influence the growth of 6T (Pithan *et al.*, 2015).

6T in the mixtures seems to grow in a very similar way to the pure films. However, the C_{60} phase influences the growth scenario in such a way that the overall dominating 6T phase is promoted even more. This means that at 303 K substrate temperature the mixtures show fewer features corresponding to the LT phase with increasing amount of C_{60}, compared to pure 6T (Figs. 7*a* and 7*c*). At 373 K, the picture is quite different. Here, the mixtures exhibit more features of the LT phase and the 6T β phase is suppressed. For the 373 K films, C_{60} seems to support the nucleation of the stable 6T LT phase (Fig. 7*e*). On the other hand, at 303 K the C_{60} phase seems to block the process by which 6T reaches the energetically stable LT phase and locks 6T in the kinetically favoured β phase. The thermal energy from the substrate which is needed to overcome the activation energy for the transition to the LT phase is partially available in the pure 6T 303 K film. However, in the 303 K mixtures the transition to the LT phase is not observed, indicating that, probably because of the presence of C_{60}, a higher transition energy is necessary.

From the real-time measurements during growth, we have seen that the growth scenario for all mixing ratios at 373 K is very similar. 6T starts to form coherently scattering domains close to the substrate (the first 2 nm of the film growth). At the beginning, these domains consist mainly of the β phase. After a certain thickness is reached, a transformation from the β phase to the LT phase takes place. Interestingly, this transformation starts at a thickness which corresponds to the nominal second monolayer of 6T. A similar transformation is not observed for pure 6T. There, at a substrate temperature of 373 K the β phase continues to nucleate throughout the whole growth process, although more slowly than the LT phase after a certain critical film thickness (around 7 nm) (Lorch *et al.*, 2015). This supports the idea that the presence of C_{60} promotes nucleation of 6T in the more stable LT phase, which

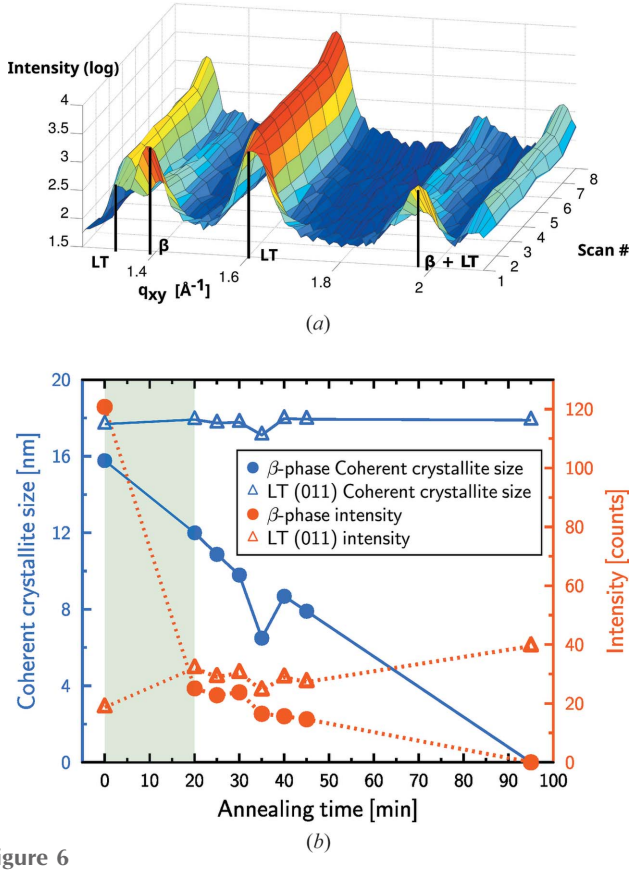

Figure 6
(*a*) Real-time GIXD scans during the annealing of the pure 6T 303 K film. The time differences between the scan numbers were not constant. A detailed description of the time steps and temperatures is given in the text. (*b*) Evolution of the β and LT phases during the annealing process as a function of time. The light blue shaded area highlights the timespan during which the heating from 303 to 373 K took place. The filled dots and open triangles represent the β and the LT phase, respectively. For the β phase the peak at $q_{xy} = 1.38$ Å^{-1} and for the LT phase the 011 peak ($q_{xy} = 1.31$ Å^{-1}) were considered. The blue solid line relates to the left *y* axis ($D_{coh||}$), and the red dashed line relates to the right *y* axis (intensity). Note that the 0 values for the β phase indicate that the peak vanished completely. The theoretical resolution limit of the setup at the LT 011 peak position is 18.7 nm, which is very close the measured result. Hence, $D_{coh||}$ of the LT 011 peak might be larger.

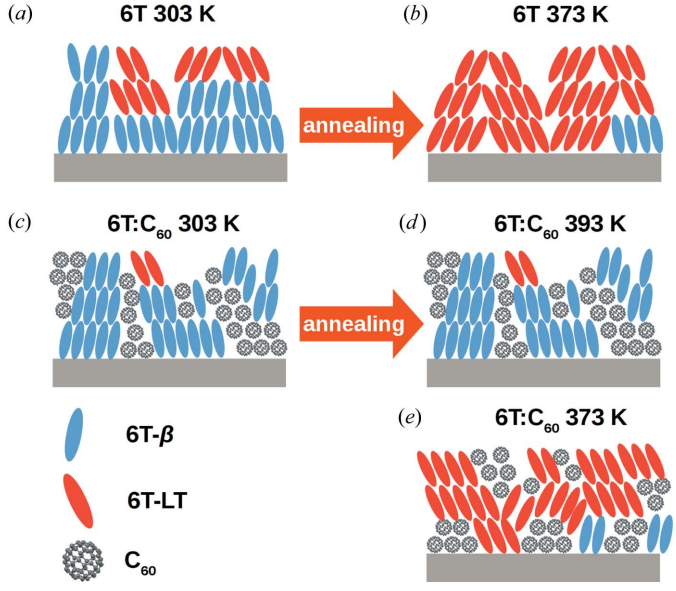

Figure 7
Schematic of the different scenarios reported. (*a*) Pure 6T prepared at 303 K with the β phase dominant close to the substrate and some LT domains in the late state of growth. (*b*) The annealed pure 6T film in which most of the β domains have been transformed to the LT phase. (*c*) 6T:C_{60} 1:1 mixture prepared at 303 K, in which the fraction of β-phase domains is higher than in the pure 6T film. (*d*) The 6T:C_{60} 1:1 mixture annealed to 393 K with no changes compared to the film as grown. (*e*) The 6T:C_{60} 1:1 mixture prepared at 373 K with the LT phase dominating the structure.

is not possible in the pure material, since the β-phase domains are attached to the substrate and hence locked in this phase.

The annealing experiments on pure 6T and 6T:C_{60} (1:1) mixtures revealed a further influence of C_{60} in the mixture. For pure 6T, the additional thermal energy put into the system *via* the annealing process leads to nucleation of 6T in the energetically stable LT phase (Figs. 7*a* and 7*b*). With enough annealing time almost all β-phase domains can be transformed into the LT phase. This leads to films consisting almost entirely of the LT phase. A similar effect is reported for H_2-phthalocyanines (H_2-Pc), where a metastable α phase (dominant for deposition at room temperature) is transformed into a more stable and more compact β phase upon annealing (Bayliss *et al.*, 1999; Heutz *et al.*, 2000; Yim *et al.*, 2002). For 6T films prepared at 373 K, there are still fractions of the β phase observed. It seems that β-phase domains created on a high-temperature substrate are stable and more difficult to convert to the LT phase.

For the annealing of 6T:C_{60} (1:1), the result is significantly different. Here, no transformation of the β phase to the LT phase is observed (Figs. 7*c* and 7*d*). The C_{60} molecules could be filling the voids between the 6T domains and acting as kinetic traps, hindering the formation of the LT phase.

This finding is similar for mixtures of pentacene (PEN) and C_{60} on nSiO, for which no changes were observed upon annealing (Salzmann *et al.*, 2008). However, for the same system when a thin PEN templating layer is employed (which usually improves the C_{60} crystallinity), an improvement of the C_{60} structure upon annealing but no changes of the PEN microstructure have been reported (Salzmann *et al.*, 2008). For pure 6T, there are some LT domains in the film, which is not the case for the mixture (see Fig. 2). It could also be that LT domains as nucleation points are necessary to promote the transition from the β to the LT phase. Furthermore, stronger coupling between the different materials might also be a reason why the transition to the LT phase is not observed, similar to results reported for an overlayer of H_2-Pc on perylenetetracarboxylic dianhydride (Heutz *et al.*, 2003).

4. Conclusion

We have investigated mixed thin films of 6T:C_{60} with nominal mixing ratios of 3:1, 1:1 and 1:3, prepared at 303 and 373 K substrate temperatures, using real-time *in situ* X-ray techniques. We observed significant differences in the crystallinity of the films prepared at the different substrate temperatures. The mixtures deposited at 303 K show overall a less pronounced crystallinity and the films are dominated by the kinetically favoured β crystal phase of 6T. In contrast, the films prepared at 373 K show a high crystallinity, consisting almost completely of standing-up crystallites of the 6T LT phase, which is energetically more stable but kinetically suppressed. We believe that C_{60} influences the film growth since the energetic landscape is different owing to the presence of C_{60} molecules.

Furthermore, annealing of pure 6T revealed remarkable changes in the film structure. These annealed films showed only features of the LT phase and no indications of the β phase were found, whereas pure 6T films prepared and measured at the same substrate temperature as the annealing temperature (373 K) still showed features of the β phase. Obviously, the kinetics of the film formation process play an important role and the domains of the β phase seem to be more robust when prepared at elevated substrate temperature. Annealing of 6T:C_{60} (1:1) films did not produce any drastic changes of the film structure or any improvement of it. This can also be attributed to the influence of C_{60}. The presence of C_{60}, filling the voids in between the 6T crystallites, might block the movement of the 6T molecules, prohibiting a transformation of the crystal structure. On the other hand, in the films prepared at 303 K the 6T LT phase is suppressed owing to the influence of C_{60}, and domains of the 6T LT phase might be needed as nucleation points for the transformation from the β phase into the LT phase.

This behaviour shows strongly that post-growth annealing of mixtures has a much weaker influence on the film structure compared to the growth on a heated substrate. After growth the energy barrier for reorganization of crystallites might be too high to be thermally overcome before the desorption point is reached.

Acknowledgements

We gratefully acknowledge the ESRF for providing us with beamtime and the staff from the ID03 beamline for their great support. This work was supported by the German Research Foundation (DFG) and by the Baden-Württemberg Stiftung in the programme 'Organic Photovoltaics and Dye Sensitized Solar Cells'. CL thanks the Carl-Zeiss-Stiftung for funding. KB acknowledges funding by the DFG (BR 4869/1-1).

References

Adams, G. B., Page, J. B., Sankey, O. F., Sinha, K., Menendez, J. & Huffman, D. R. (1991). *Phys. Rev. B*, **44**, 4052–4055.
Alem, S., Pandey, A. K., Unni, K. N. N., Nunzi, J.-M. & Blanchard, P. (2006). *J. Vac. Sci. Technol. A*, **24**, 645–648.
Als-Nielsen, J. & McMorrow, D. (2011). *Elements of Modern X-ray Physics*, 2nd ed. Chichester: John Wiley and Sons.
Aufderheide, A., Broch, K., Novák, J., Hinderhofer, A., Nervo, R., Gerlach, A., Banerjee, R. & Schreiber, F. (2012). *Phys. Rev. Lett.* **109**, 156102.
Banerjee, R., Novák, J., Frank, C., Lorch, C., Hinderhofer, A., Gerlach, A. & Schreiber, F. (2013). *Phys. Rev. Lett.* **110**, 185506.
Bayliss, S. M., Heutz, S., Rumbles, G. & Jones, T. S. (1999). *Phys. Chem. Chem. Phys.* **1**, 3673–3676.
Bommel, S., Kleppmann, N., Weber, C., Spranger, H., Schäfer, P., Novak, J., Roth, S., Schreiber, F., Klapp, S. & Kowarik, S. (2014). *Nat. Commun.* **5**, 5388.
Broch, K., Aufderheide, A., Raimondo, L., Sassella, A., Gerlach, A. & Schreiber, F. (2013). *J. Phys. Chem. C*, **117**, 13952–13960.
Broch, K., Gerlach, A., Lorch, C., Dieterle, J., Novák, J., Hinderhofer, A. & Schreiber, F. (2013). *J. Chem. Phys.* **139**, 174709.
Brock, J., Ferguson, J. & Woll, A. (2010). *Metall. Mater. Trans. A*, **41**, 1162–1166.
Brütting, W. & Adachi, C. (2012). *Physics of Organic Semiconductors*, 2nd ed. Weinheim: Wiley VCH-Verlag.
Chen, W., Zhang, H., Huang, H., Chen, L. & Wee, A. T. S. (2008). *ACS Nano*, **2**, 693–698.
Deibel, C. & Dyakonov, V. (2010). *Rep. Prog. Phys.* **73**, 096401.

Desai, T., Hong, S., Woll, A., Hughes, K., Kaushik, A., Clancy, P. & Engstrom, J. (2011). *J. Chem. Phys.* **134**, 224702.

Djuric, T., Hernandez-Sosa, G., Schwabegger, G., Koini, M., Hesser, G., Arndt, M., Brinkmann, M., Sitter, H., Simbrunner, C. & Resel, R. (2012). *J. Mater. Chem.* **22**, 15316–15325.

Drnec, J., Zhou, T., Pintea, S., Onderwaater, W., Vlieg, E., Renaud, G. & Felici, R. (2014). *J. Appl. Cryst.* **47**, 365–377.

Forrest, S. R. (2004). *Nature*, **428**, 911–918.

Haber, T., Ivanco, J., Ramsey, M. & Resel, R. (2008). *J. Cryst. Growth*, **310**, 101–109.

Hamilton, R., Shuttle, C. G., O'Regan, B., Hammant, T. C., Nelson, J. & Durrant, J. R. (2010). *J. Phys. Chem. Lett.* **1**, 1432–1436.

Heinemeyer, U., Broch, K., Hinderhofer, A., Kytka, M., Scholz, R., Gerlach, A. & Schreiber, F. (2010). *Phys. Rev. Lett.* **104**, 257401.

Heutz, S., Bayliss, S. M., Middleton, R. L., Rumbles, G. & Jones, T. S. (2000). *J. Phys. Chem. B*, **104**, 7124–7129.

Heutz, S., Salvan, G., Jones, T. S. & Zahn, D. R. T. (2003). *Adv. Mater.* **15**, 1109–1112.

Hinderhofer, A., Gerlach, A., Broch, K., Hosokai, T., Yonezawa, K., Kato, K., Kera, S., Ueno, N. & Schreiber, F. (2013). *J. Phys. Chem. C*, **117**, 1053–1058.

Hinderhofer, A., Gerlach, A., Kowarik, S., Zontone, F., Krug, J. & Schreiber, F. (2010). *Euro Phys. Lett.* **91**, 56002.

Hinderhofer, A., Hosokai, T., Yonezawa, K., Gerlach, A., Kato, K., Broch, K., Frank, C., Novák, J., Kera, S., Ueno, N. & Schreiber, F. (2012). *Appl. Phys. Lett.* **101**, 033307.

Hinderhofer, A. & Schreiber, F. (2012). *ChemPhysChem*, **13**, 628–643.

Hörmann, U., Lorch, C. *et al.* (2014). *J. Phys. Chem. C*, **118**, 26462–26470.

Hörmann, U., Wagner, J., Gruber, M., Opitz, A. & Brütting, W. (2011). *Phys. Status Solidi RRL*, **5**, 241–243.

Horowitz, G., Bachet, B., Yassar, A., Lang, P., Demanze, F., Fave, J.-L. & Garnier, F. (1995). *Chem. Mater.* **7**, 1337–1341.

Itaka, K., Yamashiro, M., Yamaguchi, J., Haemori, M., Yaginuma, S., Matsumoto, Y., Kondo, M. & Koinuma, H. (2006). *Adv. Mater.* **18**, 1713–1716.

Jones, A. O. F., Chattopadhyay, B., Geerts, Y. H. & Resel, R. (2016). *Adv. Funct. Mater.* **26**, 2233–2255.

Kiessig, H. (1931). *Ann. Phys.* **402**, 769–778.

Kowarik, S., Gerlach, A. & Schreiber, F. (2008). *J. Phys. Condens. Matter*, **20**, 184005.

Kowarik, S., Gerlach, A., Sellner, S., Schreiber, F., Cavalcanti, L. & Konovalov, O. (2006). *Phys. Rev. Lett.* **96**, 125504.

Krätschmer, W., Lamb, L. D., Fostiropoulos, K. & Huffman, D. R. (1990). *Nature*, **347**, 354–358.

Krause, B., Schreiber, F., Dosch, H., Pimpinelli, A. & Seeck, O. H. (2004). *Europhys. Lett.* **65**, 372–378.

Liscio, F., Albonetti, C., Broch, K., Shehu, A., Quiroga, S. D., Ferlauto, L., Frank, C., Kowarik, S., Nervo, R., Gerlach, A., Milita, S., Schreiber, F. & Biscarini, F. (2013). *ACS Nano*, **7**, 1257–1264.

Lorch, C., Banerjee, R., Frank, C., Dieterle, J., Hinderhofer, A., Gerlach, A. & Schreiber, F. (2015). *J. Phys. Chem. C*, **119**, 819–825.

Moser, A., Salzmann, I., Oehzelt, M., Neuhold, A., Flesch, H.-G., Ivanco, J., Pop, S., Toader, T., Zahn, D. R., Smilgies, D.-M. & Resel, R. (2013). *Chem. Phys. Lett.* **574**, 51–55.

Moulin, J.-F., Dinelli, F., Massi, M., Albonetti, C., Kshirsagar, R. & Biscarini, F. (2006). *Nucl. Instrum. Methods Phys. Res. Sect. B*, **246**, 122–126.

Nolasco, J. C., Sánchez-Díaz, A., Cabré, R., Ferré-Borrull, J., Marsal, L. F., Palomares, E. & Pallarès, J. (2010). *Appl. Phys. Lett.* **97**, 013305.

Nothaft, M. & Pflaum, J. (2008). *Phys. Status Solidi (b)*, **245**, 788–792.

Opitz, A., Wagner, J., Brütting, W., Salzmann, I., Koch, N., Manara, J., Pflaum, J., Hinderhofer, A. & Schreiber, F. (2010). *IEEE J. Sel. Top. Quant.* **16**, 1707.

Peumans, P., Uchida, S. & Forrest, S. R. (2003). *Nature*, **425**, 158–162.

Pithan, L., Cocchi, C., Zschiesche, H., Weber, C., Zykov, A., Bommel, S., Leake, S. J., Schfer, P., Draxl, C. & Kowarik, S. (2015). *Cryst. Growth Des.* **15**, 1319–1324.

Pivrikas, A., Sariciftci, N. S., Juška, G. & Österbacka, R. (2007). *Prog. Photovolt. Res. Appl.* **15**, 677–696.

Poelking, C., Tietze, M., Elschner, C., Olthof, S., Hertel, D., Baumeier, B., Würthner, F., Meerholz, K., Leo, K. & Andrienko, D. (2015). *Nat. Mater.* **14**, 434–439.

Ponchut, C., Rigal, J. M., Clément, J., Papillon, E., Homs, A. & Petitdemange, S. (2011). *J. Instrum.* **6**, C01069.

Prabakaran, R., Kesavamoorthy, R., Reddy, G. & Xavier, F. (2002). *Phys. Status Solidi (b)*, **229**, 1175–1186.

Rand, B. P., Xue, J., Uchida, S. & Forrest, S. R. (2005). *J. Appl. Phys.* **98**, 124902.

Ritley, K. A., Krause, B., Schreiber, F. & Dosch, H. (2001). *Rev. Sci. Instrum.* **72**, 1453–1457.

Rivnay, J., Mannsfeld, S. C. B., Miller, C. E., Salleo, A. & Toney, M. F. (2012). *Chem. Rev.* **112**, 5488–5519.

Roobol, S., Onderwaater, W., Drnec, J., Felici, R. & Frenken, J. (2015). *J. Appl. Cryst.* **48**, 1324–1329.

Sakai, J., Taima, T. & Saito, K. (2008). *Org. Electron.* **9**, 582–590.

Sakai, J., Taima, T., Yamanari, T. & Saito, K. (2009). *Solar Energy Mater. Solar Cells*, **93**, 1149–1153.

Salzmann, I., Duhm, S., Opitz, R., Johnson, R. L., Rabe, J. P. & Koch, N. (2008). *J. Appl. Phys.* **104**, 114518.

Scherrer, P. (1918). *Nachr. Ges. Wiss. Göttingen Math-Phys. Kl.* **1918**, 98–100.

Schreiber, F. (2004). *Phys. Status Solidi (a)*, **201**, 1037–1054.

Servet, B., Horowitz, G., Ries, S., Lagorsse, O., Alnot, P., Yassar, A., Deloffre, F., Srivastava, P. & Hajlaoui, R. (1994). *Chem. Mater.* **6**, 1809–1815.

Servet, B., Ries, S., Trotel, M., Alnot, P., Horowitz, G. & Garnier, F. (1993). *Adv. Mater.* **5**, 461–464.

Siegrist, T., Fleming, R., Haddon, R., Laudise, R., Lovinger, A., Katz, H., Bridenbaugh, P. & Davis, D. (1995). *J. Mater. Res.* **10**, 2170–2173.

Simbrunner, C., Hernandez-Sosa, G., Oehzelt, M., Djuric, T., Salzmann, I., Brinkmann, M., Schwabegger, G., Watzinger, I., Sitter, H. & Resel, R. (2011). *Phys. Rev. B*, **83**, 115443.

Singh, T. B., Sariciftci, N. S., Yang, H., Yang, L., Plochberger, B. & Sitter, H. (2007). *Appl. Phys. Lett.* **90**, 213512.

Tsutsui, T. & Fujita, K. (2002). *Adv. Mater.* **14**, 949–952.

Veenstra, S., Malliaras, G., Brouwer, H., Esselink, F., Krasnikov, V., van Hutten, P., Wildeman, J., Jonkman, H., Sawatzky, G. & Hadziioannou, G. (1997). *Synth. Met.* **84**, 971–972.

Wagner, J., Gruber, M., Hinderhofer, A., Wilke, A., Bröker, B., Frisch, J., Amsalem, P., Vollmer, A., Opitz, A., Koch, N., Schreiber, F. & Brütting, W. (2010). *Adv. Funct. Mater.* **20**, 4295–4303.

Witte, G. & Wöll, C. (2004). *J. Mater. Res.* **19**, 1889–1916.

Yang, F., Shtein, M. & Forrest, S. R. (2005). *Nat. Mater.* **4**, 37–41.

Yang, J., Yan, D. & Jones, T. S. (2015). *Chem. Rev.* **115**, 5570–5603.

Yannoni, C. S., Bernier, P. P., Bethune, D. S., Meijer, G. & Salem, J. R. (1991). *J. Am. Chem. Soc.* **113**, 3190–3192.

Ye, R., Baba, M., Ohta, K. & Suzuki, K. (2010). *Solid-State Electron.* **54**, 710–714.

Yim, S., Heutz, S. & Jones, T. S. (2002). *J. Appl. Phys.* **91**, 3632.

Yim, S. & Jones, T. S. (2009). *Appl. Phys. Lett.* **94**, 021911.

Zhang, Q.-M., Yi, J.-Y. & Bernholc, J. (1991). *Phys. Rev. Lett.* **66**, 2633–2636.

Zhong, J. Q., Huang, H., Mao, H. Y., Wang, R., Zhong, S. & Chen, W. (2011). *J. Chem. Phys.* **134**, 154706.